The Astrophysical Journal, 924:6 (13pp), 2022 January 1 https://doi.org/10.3847/1538-4357/ac300e

Co-accretion + Giant Impact Origin of the Uranus System: Post-impact Evolution

Julien Salmon and Robin M. Canup
Southwest Research Institute, Planetary Science Directorate, 1050 Walnut Street, Suite 300, Boulder, CO 80302, USA; julien@boulder.swri.edu
Received 2021 April 1; revised 2021 October 4; accepted 2021 October 12; published 2022 January 4

Abstract

We investigate aspects of the co-accretion + giant impact scenario proposed by Morbidelli et al. (2012) for the origin of the Uranian satellites. In this model, a regular satellite system formed during gas accretion is impulsively destabilized by a Uranus-tipping impact, producing debris that ultimately re-orients to the planet's new equatorial plane and re-accumulates into Uranus' current large moons. We first investigate the nodal randomization of a disk of debris resulting from disruptive collisions between the hypothesized prior satellites. Consistent with Morbidelli et al., we find that an impact-generated interior c-disk with mass $\geqslant 10^{-2}$ Uranus masses is needed to cause sufficient nodal randomization to appropriately realign the outer debris disk. We then simulate the reaccumulation of the outer debris disk into satellites and find that disks with larger initial radii are needed to produce an outer debris disk that extends to Oberon's distance, and that Uranus' obliquity prior to the giant impact must have been substantial, $\geqslant 40°$, if its original co-accreted satellite system was broadly similar in radial scale to those at Jupiter and Saturn today. Finally, we explore the subsequent evolution of a massive, water-dominated inner c-disk as it condenses, collisionally spreads, and spawns new moons beyond the Roche limit. We find that intense tidal dissipation in Uranus (i.e., $(Q/k_2)_U \leqslant 10^2$) is needed to prevent large icy moons spawned from the inner disk from expanding beyond the synchronous orbit, where they would be long lived and inconsistent with the lack of massive inner moons at Uranus today. We conclude that while a co-accretion + giant impact is viable it requires rather specific conditions.

Unified Astronomy Thesaurus concepts: Uranian satellites (1750); Computational methods (1965)

1. Introduction

The origin of the Uranian satellite system remains poorly understood. To first order, the system of the four outer major moons (Ariel, Umbriel, Titania, and Oberon) resembles the one found at Jupiter. Both systems have a total mass of about 10^{-4} times that of the planet, span a region out to ≈25 planetary radii, and have eccentricities of order 10^{-3} and inclinations of a few tenths of a degree. These traits suggest that the Uranian and Galilean satellites may have shared a common mode of origin, perhaps forming within a circumplanetary disk produced during gas co-accretion. For example, Canup & Ward (2006) proposed that gas inflow to a giant planet preferentially selects for a satellite system with a mass of about 10^{-4} times that of the planet, and that such a system could have been generated during the accretion of Uranus' gas component, even though the latter comprises only of order 10% of the planet's mass. While diverse models of satellite co-accretion during gas inflow have been subsequently developed (e.g., Ogihara & Ida 2012; Cilibrasi et al. 2018, 2021; Drążkowska & Szulágyi 2018; Shibaike et al. 2019; Batygin & Morbidelli 2020; Fujii & Ogihara 2020; Ronnet & Johansen 2020), recent population synthesis models continue to find a strong preference for satellite systems with mass ratios at or below $\sim 10^{-4}$ (Cilibrasi et al. 2021). The four major Uranian moons contain about half rock and half ice, which is also consistent with solar composition material expected in a relatively cool co-accreting circumuranian disk (e.g., Canup & Ward 2006). However, gas inflow would produce a prograde disk with respect to Uranus' orbit around the Sun (e.g., Lubow et al. 1999). Thus, co-accretion alone would produce a satellite system orbiting in the opposite sense to that observed.

Newly formed Uranus may have had a smaller obliquity and a prograde rotation, with its current retrograde state due to a later event. A spin–orbit resonance could have raised Uranus' obliquity significantly, though achieving its current 98° value does not appear possible via this mechanism alone (Rogoszinski & Hamilton 2020). Instead, Uranus' current obliquity may be due to a giant impact by a roughly Earth-sized projectile. This impact could have also produced a disk and satellites orbiting in the same sense as Uranus' retrograde rotation (Slattery et al. 1992; Ida et al. 2020). However, impacts produce disks that are generally rock-poor by mass and more radially compact than Uranus' outer moons (e.g., Slattery et al. 1992; Reinhardt et al. 2020; Rufu & Canup 2020). The former seems at odds with the Uranus moon compositions. Moons spawned from a compact disk could tidally evolve outward (Crida & Charnoz 2012), but explaining outer Oberon requires a tidal expansion rate averaged over the system lifetime that is orders-of-magnitude faster than inferred from the resonant excitation of Miranda's orbital inclination (Tittemore & Wisdom 1990). Alternatively, it has been suggested that rocky solids were transported outward over large distances as an impact-generated disk's water vapor viscously expanded, increasing the rock-to-ice ratio in the satellite forming region compared to that in the initial disk (Ida et al. 2020).

A promising alternative was proposed by Morbidelli et al. (2012), who suggested that the current situation at Uranus could be the result of a combination of both the co-accretion and giant impact concepts. In their scenario, Uranus originally had a non-negligible prograde obliquity of ∼10°–30°, which could be the result of prior impacts and/or a spin–orbit resonance (Rogoszinski & Hamilton 2020), and a satellite system of mass $\sim 10^{-4} M_U$ (where M_U is Uranus' current mass),

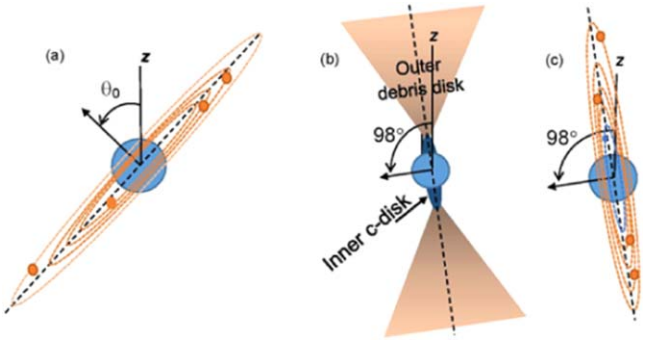

Figure 1. Co-accretion + giant impact concept of Morbidelli et al. (2012). Dashed lines indicate Uranus' equatorial plane, while the z-axis is normal to Uranus' orbital plane. (a) Uranus begins with a prograde obliquity (θ_0) and a satellite system with mass $\sim 10^{-4} M_U$, likely formed by co-accretion. A giant impact then creates Uranus' 98° obliquity and an inner c-disk with mass $\sim 10^{-2} M_U$. The impact's impulse destabilizes the prior moons, causing initially disruptive mutual collisions. (b) Debris from these collisions is forced (primarily) by the equatorial c-disk to differentially precess, producing an outer debris torus with mass $\sim 10^{-4} M_U$ that is symmetric about Uranus's new equatorial plane. Inelastic collisions among debris material flatten the torus into an equatorial disk. (c) Uranus' current large satellites with total mass $\sim 10^{-4} M_U$ re-accrete from the outer debris disk on low-inclination orbits relative to the planet's final equatorial plane (orange), while the much more massive c-disk and nearly all of its byproducts (blue) must ultimately be lost to collision with Uranus.

likely produced by co-accretion during Uranus' limited gas accretion phase. A giant impact then tilts the planet to its current 98° obliquity, and impulsively perturbs the preexisting satellites into mutually crossing orbits.

Disruptive collisions between the satellites are then postulated to produce a debris disk in the *pre-impact* equatorial plane of the planet. This disk is initially highly tilted relative to Uranus' new, *post-impact* equatorial plane. The planet's oblateness (primarily its J_2) causes the ascending nodes of disk material to precess about the planet's new equatorial plane, with precession rates that vary strongly with distance. If the planet's J_2 were the only source of precession, the ascending nodes of outer debris orbits would quickly randomize, with the initially highly inclined debris *ring* evolving into a thick torus symmetric about the planet's new equatorial plane. Inelastic collisions within the torus would damp relative vertical motions, leading to an equatorial disk and ultimately low-inclination satellites. If only a minority of debris were lost to escape or collision with the planet, the final satellite system would then approximately preserve the 10^{-4} satellite system mass ratio produced by Uranus' earlier gas accretion.

This desired outcome is frustrated by the gravity of the outer debris disk itself, which tries to force its material to precess about its initial plane. This effect dominates over that of the planet's J_2 at distances beyond about $7R_U$ (where R_U is Uranus' current mean radius), causing the outer regions of the debris disk to precess rigidly and maintain an inclined structure (Morbidelli et al. 2012). Such a warped disk would accrete into outer moons with large inclinations, inconsistent with the low inclinations of Titania and Oberon. The clever solution proposed in Morbidelli et al. (2012) recognizes that the Uranus-tilting impact itself could have created an approximately equatorial inner disk, extending to perhaps a few Uranian radii (Figure 1(b)), and the gravity of this *c-disk* would enhance the effect of the planet's J_2. For a massive enough c-disk, even the outer debris disk could then be appropriately realigned to the planet's new equatorial plane.

However, the required c-disk mass is very large, $\sim 10^{-2} M_U$, about 100 times the mass of the Uranian satellite system. A final needed step for success of the model is that the c-disk and its massive byproducts must be lost, as no comparably massive ring or inner moon exist at Uranus today. Morbidelli et al. (2012) suggested that c-disk material remained interior to the synchronous orbit (currently located at about $3.3R_U$) and was ultimately lost by inward tidal decay. However, it is unclear whether this is probable, given the tendency for moons spawned from a massive inner disk to spread substantially outward due to disk torques and mutual interactions (e.g., Salmon & Canup 2012, 2017).

In this paper, we address some key aspects of the co-accretion + giant impact model to evaluate the conditions needed for (1) the outer debris disk to accrete into a Uranian-like satellite system with low inclinations and an outermost large satellite orbit similar to that of Oberon, and (2) preservation of this re-accreted, $\sim 10^{-4} M_U$ mass satellite system as a much more massive inner c-disk later cooled and evolved.

2. Evolution of the Outer Debris Disk

We consider the evolution of the outer debris disk after the Uranus-tipping impact, and assess conditions required for it to fully realign with Uranus' new equatorial plane so as to produce a system of low-inclination moons similar to Uranus' four largest moons. We then simulate the accretion of satellites from this disk after its realignment, and evaluate basic disk properties needed to account for the current Uranian satellite system.

2.1. Nodal Randomization

We assume that the impulse to the planet from the giant impact destabilizes a prior satellite system, leading to mutually disruptive collisions that produce an outer debris disk with mass $\sim 10^{-4} M_U$. To estimate the mass of the inner c-disk needed to cause rapid nodal regression out to distances consistent with low-inclination Oberon, Morbidelli et al. (2012) used a Laplace–Lagrange ring code and an N-body code, mimicking the secular effect of an inner c-disk by treating it as a moon of mass M_c orbiting at $3R_U$ (hereafter we will refer to this body as the *c-moon*). We adopt a similar approach, but model the outer debris disk with an N-body simulation (Duncan et al. 1998) that includes inelastic collisions (adopting normal and tangential coefficients of restitution) and mergers when the rebound velocity is below a mutual escape velocity (as in Salmon & Canup 2012). The goal is to assess when nodal randomization driven by the inner c-disk overcomes the tendency for gravitational interactions among fragments in the outer disk to maintain an inclined disk.

Table 1 lists the initial parameters for our simulations. All begin with an outer disk of 5000 equal-mass particles arranged in a radially flat surface density profile, with a total outer disk mass of $10^{-4} M_U$ and with semimajor axes extending from $4–40R_U$. The initial N-body particles are large, >50 km in radius, which sets the granularity of the treatment of self-gravity in our simulations. The actual initial size of outer debris fragments is uncertain. Gravitational interactions are treated with an N^2 algorithm with mutual interactions included for bodies closer than about 6 mutual Hill radii (Duncan et al. 1998). All particles initially have the same eccentricity (0.1),

Table 1
N-body Simulations of Nodal Randomization in the Outer Debris Disk

Run	$M_{\text{c-moon}}$ (M_{U})	Ω_d (deg)	i_d (deg)	$\sigma(\Omega_{d,>30R_{\text{U}}})$ at 100 yr (deg)	$\sigma(\Omega_{d,>30R_{\text{U}}})$ at 1000 yr (deg)	$\langle e_d \rangle$	$\langle i_d \rangle$ (deg)
1	0.003	0	30	1.6	4.7	0.088	23.8
2	0.003	10	30	1.6	7.0	0.091	23.7
3	0.003	20	30	1.7	5.8	0.086	23.7
4	0.003	0	45	1.9	2.4	0.106	33.5
5	0.003	10	45	4.8	2.5	0.098	32.5
6	0.003	20	45	7.2	5.3	0.108	32.7
7	0.003	0	60	6.1	5.1	0.119	46.8
8	0.003	10	60	2.5	1.7	0.142	46.2
9	0.003	20	60	1.2	10.2	0.141	46.7
10	0.010	0	30	9.2	46.5	0.098	20.3
11	0.010	10	30	8.7	48.3	0.101	20.6
12	0.010	20	30	8.8	48.1	0.098	20.9
13	0.010	0	45	8.3	50.3	0.126	34.0
14	0.010	10	45	8.5	49.1	0.119	33.4
15	0.010	20	45	6.2	46.1	0.129	33.8
16	0.010	0	60	5.2	35.9	0.147	48.6
17	0.010	10	60	5.6	43.0	0.149	48.9
18	0.010	20	60	3.2	43.9	0.141	49.8
19	0.030	0	30	42.4	52.1	0.167	20.1
20	0.030	10	30	44.5	51.2	0.175	19.7
21	0.030	20	30	46.6	50.8	0.172	20.2
22	0.030	0	45	37.7	50.1	0.198	33.2
23	0.030	10	45	42.1	51.4	0.196	33.4
24	0.030	20	45	42.4	51.4	0.202	33.6
25	0.030	0	60	27.9	53.4	0.209	56.0
26	0.030	10	60	29.6	52.0	0.235	56.4
27	0.030	20	60	26.6	52.7	0.225	55.3

Note. Initial parameters and results from our numerical simulations of nodal randomization in the outer debris disk. $M_{\text{c-moon}}$ is the mass of the inner c-moon used to mimic the c-disk. We set its initial longitude of ascending node to 0 in all runs. Ω_d and i_d are the initial longitude of ascending node and inclination of disk particles. $\sigma(\Omega_{d,>30R_{\text{U}}})$ is the standard deviation of the longitude of ascending node of disk particles with semimajor axis beyond $30R_{\text{U}}$. We use this quantity to measure how much nodal randomization has occurred in the distant regions of the disk; randomization out to $\geqslant 30R_{\text{U}}$ is needed to successfully explain Oberon for $i_d \geqslant 30°$. $\langle e_d \rangle$ and $\langle i_d \rangle$ are the mean eccentricity and inclination of disk particles at $t = 1000$ yr. All particles have an initial mass of $2 \times 10^{-8} M_{\text{U}}$.

longitude of ascending node (either 0°, 10°, or 20°), and orbital inclinations (either 30°, 45° or 60°). The different initial inclinations correspond to different assumptions for the angle between Uranus' pre-impact and post-impact spin axes, δ, which itself is a function of the assumed value for θ_0, Uranus' pre-impact obliquity, and the azimuthal positions of the planet's spin axes before and after the impact. The angle δ must be less than 90° so that once the disk realigns with the planet's new equatorial plane, disk material will orbit in the same direction as the planet's spin as needed to yield the current satellite system. For a randomly oriented giant impact, the impact orientation needed to satisfy the $\delta < 90°$ condition becomes more probable as θ_0 is increased, with 30%–60% of orientations yielding $\delta < 90°$ for $10° \leqslant \theta_0 \leqslant 70°$ (Morbidelli et al. 2012). We identify a second, more stringent requirement that δ must be less than ~60° to account for Oberon's orbital distance if one assumes the prior satellite system orbited within 10^2 R_{U} (see Section 2.3).

The large c-moon used to mimic the effect of the c-disk in our simulations has a mass of 0.003, 0.01, or $0.03 M_{\text{U}}$, and is placed initially at $3R_{\text{U}}$ on a circular, non-inclined orbit. We set the initial longitude of ascending node of the c-moon to 0. We use normal and tangential coefficients of restitution of $\epsilon_n = 0.01$ and $\epsilon_t = 1$, similar to other studies of satellite accretion (Ida et al. 1997; Salmon & Canup 2012; Canup & Salmon 2018). We ignore precessional forcing by the Sun. For the current large Uranian moons, solar effects are minimal and the Laplacian plane is coincident with the planet's equatorial plane out to Oberon's distance (e.g., Dobrovolskis 1991). Because the simulations here also include the effect of a massive inner c-disk, the distance at which solar forcing becomes important will be larger still, and so we neglect it here.

Uranus' physical radius at the time of a late giant impact would have been somewhat larger than its current radius (with plausibly $R_p \sim 1.2$–$1.5R_{\text{U}}$; e.g., Bodenheimer & Pollack 1986; Fortney et al. 2007), and its early rotation rate slower by conservation of spin angular momentum. A slower rotation rate would decrease the planet's J_2, since $J_2 \propto \omega^2$ (e.g., Bertotti & Farinella 1990), where ω is the spin frequency of the planet. The spin angular momentum of a planet of mass M_{U} and radius R_P is $L_{\text{spin}} = k M_{\text{U}} R_P^2 \omega$, where k is the moment of inertia constant. Conservation of spin angular momentum gives $R_{\text{U}}^2 \omega_{\text{U}} = R_P^2 \omega$, where $\omega_{\text{U}} \sim 10^{-4}\ \text{s}^{-1}$ is the current spin of Uranus and we assume for simplicity an early Uranus with a moment of inertia constant comparable to that of the current planet. For an early Uranus with a radius of $R_P = 1.3R_{\text{U}}$, this yields a post-impact $\omega \sim 6.2 \times 10^{-5}\ \text{s}^{-1}$. Accordingly, we set $J_2 \sim 1.3 \times 10^{-3}$ in our simulations, about a factor of 2.6 smaller than the current J_2 of Uranus.

Figure 2 shows the node, eccentricity, and inclination of disk particles at 0, 100, and 1000 yr, for cases with a smaller c-moon ($M_c = 0.003 M_{\text{U}}$; Run 1) and a larger c-moon

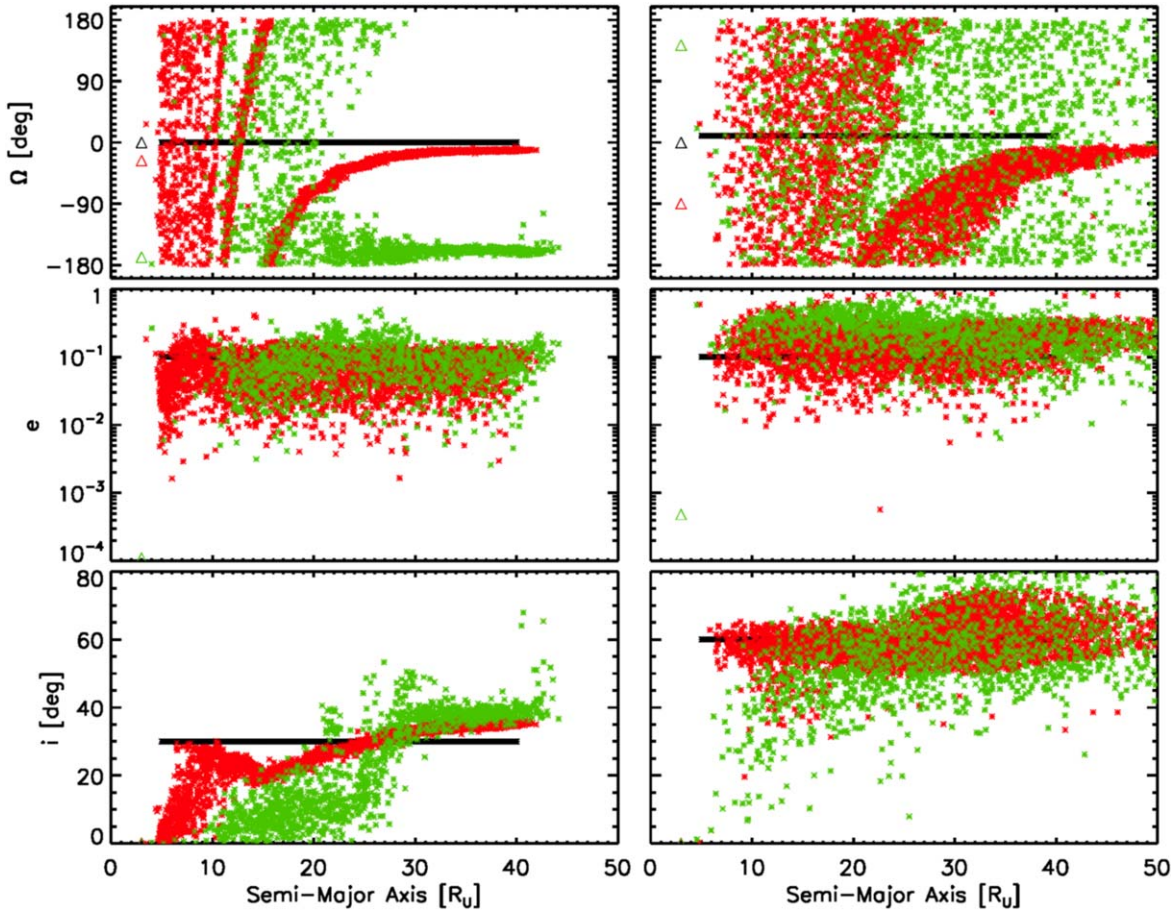

Figure 2. Nodal randomization of outer disk particles under the influence of Uranus' J_2 and a massive c-disk represented in these simulations by a large moon at $3R_U$. Left and right panels are for Runs 1 and 26, respectively. The top row shows the longitude of ascending node Ω, the middle row shows eccentricity, and the bottom row shows inclination. Black, red, and green points show the system at $t = 0$, 100, and 1000 yr; colored triangles show the c-moon at the same times of evolution.

($M_c = 0.03M_U$; Run 26). In the first, the nodes of disk particles efficiently randomize out to distances of about $20R_U$. Beyond that distance, the particles retain a common node (i.e., they are precessing coherently), indicating a warped outer disk structure that would yield an inclined outer satellite. In the case with a larger c-moon (Figure 2, right), the nodes of the particles are efficiently randomized across the entire disk after 1000 yr.

The planet's J_2 and the c-moon cause outer particle nodes to regress with a regression rate that decreases rapidly with orbital distance while producing no (direct) secular change in particle semimajor axes (a). However, as the initially tilted ring begins to regress, inner regions regress more rapidly, and this differential nodal regression produces a temporary mass distribution that is akin to a leading spiral wave pattern. Self-gravity across this structure produces a negative torque on the outer disk regions in our simulations that affects debris orbital elements (including a). The effect is short-lived, existing only prior to substantial dispersion of the nodes.

Columns 5–8 in Table 1 show several properties of the resulting outer disk particles. To quantify the efficiency of nodal randomization, we measure the standard deviation of the longitude of ascending node of disk particles located beyond $30R_U$ after 100 and 1000 yr of evolution (this quantity is initially 0 as all disk particles have the same node). We find, as expected, larger randomization for runs with a larger c-moon. For $M_c = 0.003M_U$, nodes in the 30–$40R_U$ region are minimally dispersed by $<10^\circ$ and retain coherency, while for $M_c \geqslant 0.01M_U$, nodal dispersion reaches about 50° across this region within 10^3 yr. Overall, our results agree with those of Morbidelli et al. (2012) on the c-disk mass required to realign the outer regions of the debris disk to Uranus' post-impact equatorial plane.

2.2. Post-impact Timescales

Consider the Uranus system just after a giant impact by an approximate Earth mass projectile has produced the planet's 98° obliquity and a massive c-disk. The needed c-disk would be compact, with a radius of a few R_U, and it would likely be composed predominantly of water and be (approximately) aligned with the planet's post-impact equatorial plane (Slattery et al. 1992; Reinhardt et al. 2020; Rufu & Canup 2020). The energy of the impact will have heated the planet's surface to temperatures $\sim 10^4$ K, and vaporized the c-disk. Outer debris produced by disruptive collisions among the prior satellites is expected to contain roughly half ice and half rock, consistent with expected compositions of moons accreted during Uranus' late gas co-accretion (e.g., Canup & Ward 2006). Ice may sublimate due to Uranus' luminosity, even at large distances; e.g., a rotating particle at distance r, with Bond Albedo $A_b \sim 0.1$, and emissivity $\epsilon_{ir} \sim 1$, will be heated to a temperature $T_{par} \sim [(R_U/r)^2(1 - A_b)/(4\epsilon_{ir})]^{1/4} T_U$, which for an effective temperature for Uranus of $T_U > 2000$ K implies $T_{par} > 200$ K for $(r/R_U) < 50$. Resulting water vapor thermal velocities would be less than the local escape velocity. Thus we expect

the outer disk may initially contain water vapor and (primarily) rocky debris.

With time Uranus cools, losing the heat delivered by the giant impact. To (crudely) estimate its cooling timescale, consider a case in which the impact energy, $\sim\frac{1}{2}M_{\oplus}(20\ \mathrm{km\ s^{-1}})^2 \sim 1.2\times10^{40}$ erg, is deposited in an outer layer of the planet that is heated by $\Delta T = 10^4$ K, which implies an outer layer mass $\sim 0.15 M_{\rm U}$. For comparison, an SPH simulation of the impact of a 1 Earth mass object into a Uranus-like planet with an impact velocity of 1.1 times the mutual escape velocity and a 45° impact angle heats the outer ~10% of the planet's mass by $\geqslant 10^4$ K (R. M. Canup 2017, personal communication; see also Rufu & Canup 2020). For a well-mixed layer, the time for Uranus to cool to temperature $T_{\rm U}$ is

$$t \sim \frac{0.15 M_{\rm U} C}{4\pi R_{\rm U}^2 \sigma_{\rm SB} T_{\rm U}^3}, \quad (1)$$

where $C \sim 10^8$ erg K^{-1} g^{-1} is specific heat and $\sigma_{\rm SB}$ is the Stefan–Boltzmann constant. As Uranus cools, the ice condensation distance at which $T \sim 200$ K moves inward to smaller orbital radii. An opaque vapor disk passively heated by the planet has a temperature $T \sim 0.3(3R_{\rm U}/r)^{3/4}T_{\rm U}$ (e.g., Ruden & Pollack 1991). Combining this with $T_{\rm U}(t)$ from Equation (1) provides a simple estimate of the time to ice condensation (i.e., $T \leqslant 200$ K) as a function of r. Beyond $10R_{\rm U}$, ice may condense after 10^2–10^3 yr, which is less than or comparable to the local satellite accretion timescale (see below). However, for $r \leqslant 5R_{\rm U}$ Uranus' luminosity would maintain a water-dominated c-disk as a vapor for 10^4–10^5 yr. Deeper energy deposition in the planet and/or less efficient mixing would yield slower cooling than these estimates. However in general, one expects satellite accretion in the outer debris disk would occur before the inner c-disk cools and begins to condense. Accordingly, we first model accretion in the outer debris disk (Section 2.3), and then separately consider the later viscous evolution of the inner c-disk as it starts to condense, spread, and spawn moonlets (Section 3).

2.3. Accretion in the Outer Debris Disk

We simulate the reaccumulation of the outer debris disk to identify conditions needed to yield a system broadly similar to today's Ariel, Umbriel, Titania, and Oberon in terms of satellite number, masses, and orbital distribution. We perform a suite of N-body accretion simulations, with initial disk parameters indicated in Table 2. The combined mass of Ariel, Umbriel, Titania, and Oberon is $M_{\rm AUTO} = 1.044\times10^{-4}M_{\rm U}$; we use a somewhat larger initial disk mass ($1.15\times10^{-4}M_{\rm U}$) to allow for some material loss. We consider a vapor-free disk that is roughly half rock and half ice (with a particle bulk density of 1.5 g cm^{-3}), which is plausible if Uranus cools efficiently, and neglect the gravitational potential of the c-disk, since we assume that precession forced by the planet's J_2 and the c-disk has already randomized the outer debris disk nodes.

Disk particles are assigned average starting eccentricities of 0.1 or 0.2, and initial inclinations of 30°, 45°, or 60° with random longitudes of ascending node, so that the disk is a thick torus centered on the planet's equatorial plane. We consider two surface density profiles ($\sigma(r) \propto r^{-q}$ with $q = 0$, 1), and two values for the normal coefficient of restitution ($\epsilon_N = 0.01$, 0.1). We continue the simulations for 3×10^4 yr.

Figure 3 (left) shows the evolution of the system from Run 14. Satellites grow as particles collide and merge, and this process is most rapid in the inner region of the disk because collision rates depend on orbital frequency, Ω. Consider an outer debris disk with mass $10^{-4}M_{\rm U}$ distributed uniformly out to $\sim 25R_{\rm U}$, with surface density $\sigma \sim 700$ g cm^{-2}. As the disk collisionally evolves, the balance between gravitational stirring and collisional damping will yield an equilibrium dispersion velocity, u, that is comparable to the escape velocity for the object size that contains most of the swarm's mass. The accretion timescale for a radius R body (or alternatively, the time spent at radius R) is approximately $\tau_{\rm acc} \sim (\rho R/\sigma)(f_g\Omega)^{-1}$, where ρ is the body density and f_g is a gravitational focusing factor that is a function of $(v_{\rm esc}/u)^2$, where $v_{\rm esc}$ is the escape velocity of the growing body and u is the dispersion velocity of the accreted material. If accreting objects are similar in size, or if the largest objects contain most of the system mass (as is true in the end stages of accretion), then $u \geqslant v_{\rm esc}$ and f_g is of order unity, implying growth of a $R \sim 750$ km, ice–rock satellite at $15R_{\rm U}$ in ~500 yr, consistent with our simulation results. Earlier growth could be much faster if a larger body is accreting smaller material and most of the swarm mass is contained in the smaller material, because $(v_{\rm esc}/u)$ and f_g can then be large. Our simulations are limited in their ability to resolve such effects by their numerical resolution.

After 3×10^4 yr, the simulation in Figure 3 (left) obtains a satellite system broadly similar to Ariel, Umbriel, Titania, and Oberon. However there is no low-mass Miranda analog, perhaps pointing to a different origin for this moon (see below). The outer debris disk accretion process is completed within a few 10^4 yr. Properties of the final large satellites, defined as those having a mass greater than $10^{-5}M_{\rm U}$, are shown in the right portion of Table 2. The average final number of large satellites and total satellite system mass across the simulations are $\langle N_{\rm sats}\rangle = 4.24\pm0.9$ and $\langle M_{\rm sats}/M_{\rm AUTO}\rangle = 0.95\pm0.09$, in good agreement with the current system. Disks with an initial outer edge equal to Oberon's current distance of $23R_{\rm U}$ (Runs 1–14) produce systems that are on average too radially compact, with an outermost moon well interior to Oberon's current distance ($\langle a_{\rm max}/a_{\rm Oberon}\rangle = 0.50$). Increasing the initial outer edge to $30R_{\rm U}$ (Table 2, Runs 15–22) improves this result, with $\langle a_{\rm max}/a_{\rm Oberon}\rangle = 0.77$. For both $(R_{\rm out}/R_{\rm U}) = 23$ and 30, the final systems are more compact as the initial i is increased.

The latter effect is simply understood. As an initially thick, high-i torus collisionally damps to form a flattened disk and satellites, the components of its particles' orbital angular momentum in the equatorial plane will tend to cancel out, while the components perpendicular to this plane will be approximately conserved. The latter would be $h_{\rm perp} \approx \sqrt{GM_{\rm U}a_o}\cos i$ for initial debris with inclination i, small eccentricity, and semimajor axis a_o. Conservation of this quantity as material collisionally damps to low-i orbits implies contraction to a distance $a_f \sim a_o(\cos i)^2$. Requiring a final maximum semimajor axis consistent with Oberon's distance, i.e., $a_f \approx 25R_{\rm U}$, then implies that an initial disk with a substantially larger maximum semimajor axis, $R_{\rm out} \sim 25R_{\rm U}/(\cos i)^2$, is needed, a condition most closely met by Runs 5–6, 11–14, and 19–22, whose results are (generally) the most consistent with the current Uranian satellites.

Table 2
N-body Simulations of Outer Debris Disk Accretion

Run	N	$R_{\rm out}$ ($R_{\rm U}$)	q	$\langle e_d \rangle$	$\langle i_d \rangle$ (deg)	ϵ_N	$N_{\rm sats}$	$M_{\rm sats}$ ($M_{\rm AUTO}$)	$a_{\rm min}$ ($R_{\rm U}$)	$a_{\rm max}$ ($a_{\rm Oberon}$)	$\langle e_{\rm sats} \rangle$	$\langle i_{\rm sats} \rangle$ (deg)
1	5000	23	0	0.1 ± 0.03	45 ± 3	0.01	4	0.94	4.52	0.41	0.018 ± 0.015	1.7 ± 0.35
2	5000	23	1	0.1 ± 0.03	45 ± 3	0.01	5	0.93	2.97	0.41	0.012 ± 0.006	1.4 ± 0.09
3	5000	23	0	0.2 ± 0.03	60 ± 3	0.01	2	0.91	3.45	0.21	0.025 ± 0.004	2.0 ± 0.22
4	5000	23	1	0.2 ± 0.03	60 ± 3	0.01	4	0.82	2.54	0.20	0.003 ± 0.003	2.0 ± 0.13
5	5000	23	0	0.1 ± 0.03	30 ± 3	0.01	4	0.93	6.70	0.65	0.016 ± 0.011	0.6 ± 0.41
6	5000	23	1	0.1 ± 0.03	30 ± 3	0.01	6	1.10	3.82	0.71	0.042 ± 0.020	1.7 ± 0.86
7	5000	23	0	0.1 ± 0.03	45 ± 3	0.1	3	0.91	5.59	0.43	0.006 ± 0.003	1.1 ± 0.27
8	5000	23	1	0.1 ± 0.03	45 ± 3	0.1	5	0.93	3.59	0.39	0.015 ± 0.006	1.3 ± 0.42
9	5000	23	0	0.2 ± 0.03	60 ± 3	0.1	4	1.03	1.92	0.20	0.028 ± 0.008	1.8 ± 0.52
10	5000	23	1	0.2 ± 0.03	60 ± 3	0.1	4	0.86	2.41	0.23	0.007 ± 0.003	2.0 ± 0.04
11	5000	23	0	0.1 ± 0.03	30 ± 3	0.1	4	0.96	7.19	0.68	0.007 ± 0.004	0.8 ± 0.21
12	5000	23	1	0.1 ± 0.03	30 ± 3	0.1	4	1.03	4.06	0.63	0.027 ± 0.012	0.7 ± 0.21
13	1000	23	0	0.1 ± 0.03	10 ± 3	0.1	4	0.99	8.89	0.94	0.021 ± 0.018	0.3 ± 0.12
14	1000	23	1	0.1 ± 0.03	10 ± 3	0.1	4	0.91	8.66	0.97	0.030 ± 0.019	0.9 ± 0.47
15	1500	30	0	0.1 ± 0.03	45 ± 3	0.1	4	0.96	6.67	0.65	0.018 ± 0.006	2.3 ± 0.25
16	1500	30	1	0.1 ± 0.03	45 ± 3	0.1	6	1.04	3.47	0.59	0.014 ± 0.002	2.2 ± 0.48
17	1500	30	0	0.2 ± 0.03	60 ± 3	0.1	5	1.01	2.98	0.31	0.007 ± 0.002	4.2 ± 0.28
18	1500	30	1	0.2 ± 0.03	60 ± 3	0.1	4	0.73	3.52	0.28	0.007 ± 0.006	4.1 ± 0.24
19	1500	30	0	0.1 ± 0.03	30 ± 3	0.1	4	0.88	11.75	1.07	0.014 ± 0.008	1.4 ± 0.59
20	1500	30	1	0.1 ± 0.03	30 ± 3	0.1	4	1.00	5.62	0.79	0.050 ± 0.019	1.5 ± 0.51
21	1500	30	0	0.1 ± 0.03	10 ± 3	0.1	5	1.08	7.52	1.35	0.069 ± 0.029	1.8 ± 0.86
22	1500	30	1	0.1 ± 0.03	10 ± 3	0.1	4	0.87	10.28	1.13	0.030 ± 0.008	0.7 ± 0.51

Note. Results from *N*-body simulations of satellite accretion in the outer debris disk. All disks have an initial disk mass $M_d = 1.15 \times 10^{-4} M_{\rm U}$, and contain N particles distributed with a surface density profile $\sigma \propto a^{-q}$. $R_{\rm out}$ is the semimajor axis of the outermost particles, and $\langle e_d \rangle$ and $\langle i_d \rangle$ are the mean eccentricities and inclination of the disk particles at the beginning of the simulation. ϵ_N is the normal coefficient of restitution used when treating collisions between particles. $N_{\rm sats}$ is the number of large satellites at $t = 3 \times 10^4$ yr, where we define large as having a mass greater than $10^{-5} M_{\rm U}$. $M_{\rm sats}$ is the total mass of large satellites in units of the combined mass of Ariel, Umbriel, Titania, and Oberon $M_{\rm AUTO}$. $a_{\rm min}$ and $a_{\rm max}$ are the semimajor axes of the innermost and outermost final large satellites in units of $R_{\rm U}$ and the current semimajor axis of Oberon $a_{\rm Oberon}$, respectively. $\langle e_{\rm sats} \rangle$ and $\langle i_{\rm sats} \rangle$ are the mean eccentricities and inclination of the final large satellites.

This constraint has implications for the needed giant impact configuration. Just after the giant impact and prior to substantial collisional inclination damping, the outer debris disk inclination relative to Uranus' new, post-impact equatorial plane would have been $\approx \delta$, the angle between Uranus' pre-impact and post-impact spin axes. The initial $R_{\rm out}$ value for this debris would have been comparable to the outer radius of the preexisting regular satellite system formed by co-accretion. Requiring $a_f \approx 25 R_{\rm U}$ to account for Oberon then constrains δ, with $\delta = \cos^{-1}[(25 R_{\rm U}/R_{\rm out})^{1/2}]$. It seems reasonable to assume that a preexisting Uranian satellite system formed via co-accretion would have had a broadly comparable radial scale to that of the Jovian and Saturnian regular satellites, with an outermost large satellite interior to 100 planetary radii. For $R_{\rm out} \leqslant 100 R_{\rm U}$, the maximum allowable value for δ is then 60° if one requires $a_f \approx 25 R_{\rm U}$. Together with the requirement that the giant impact leave Uranus with its current 98° obliquity, this means that Uranus' obliquity prior to the giant impact in the Morbidelli et al. (2012) scenario must have been substantial, with $\theta_0 \sim 40°$ or greater. This may not be implausible, given Neptune's 30° obliquity and the possibility for multiple large impacts and/or spin–orbit resonant effects (Rogoszinski & Hamilton 2020), but it is more restrictive than the arguments advanced in Morbidelli et al. (2012), which considered only the $\delta < 90°$ constraint cited in Section 2.1 that allows for smaller values of θ_0.

The Table 2 simulations produced on average an innermost large satellite well interior to Ariel, with $\langle a_{\rm min}/R_{\rm U} \rangle = 5.4 \pm 2.8$ versus $(a_{\rm Ariel}/R_{\rm U}) = 7.5$. Our first suite of simulations retained all objects that avoided direct collision with the planet. However, objects that strayed within a few $R_{\rm U}$ may instead have been lost due to gas drag by the inner water vapor c-disk. A c-disk with mass $10^{-2} M_{\rm U}$ that extends from the planet's surface to $3 R_{\rm U}$ has a surface density $\sigma \sim 6 \times 10^6$ g cm^{-2}. The lifetime of a satellite with radius R and density ρ orbiting within such a disk is

$$\tau_{\rm gd} \sim \frac{8}{3 C_D} \frac{\rho R}{\sigma} \left(\frac{r\Omega}{c} \right)^3 \Omega^{-1}, \quad (2)$$

where $C_D \sim O(1)$ is a drag constant, and $c/(r\Omega)$ is the vapor scale height of the disk, where c is the vapor sound speed, which is few $\times 10^5$ cm s^{-1} soon after the impact (Rufu & Canup 2020). Near $3 R_{\rm U}$, the loss timescale may then be only

$$\tau_{\rm gd} \sim 10 \text{ yr} \quad (1/C_D) \quad (6 \times 10^6 \text{ g cm}^{-2}/\sigma)(R/500 \text{ km})(0.1/[c/r\Omega])^3.$$

As such, we repeated a subset of the runs with the condition that any object that strayed within $3 R_{\rm U}$ was removed; results are shown in Table 3 and in Figure 3 (right). The average number and total mass of large satellites in these runs are $\langle N_{\rm sats} \rangle = 3.47 \pm 1.2$ and $\langle M_{\rm sats}/M_{\rm AUTO} \rangle = 0.79 \pm 0.28$, while the average semimajor axis of the innermost final large satellite is increased to $\langle a_{\rm min}/R_{\rm U} \rangle = 5.69 \pm 1.58$, in somewhat better agreement with Ariel. However, we still do not see Miranda analogs: the final innermost moons in these simulations all have masses more than 15 times that of Miranda.

Inner Miranda is distinct not just because of its much smaller mass compared with the outer large moons, but also because of its apparent composition. The large moons have similar densities between 1.52 and 1.66 g cm^{-3} (Jacobson 2014),

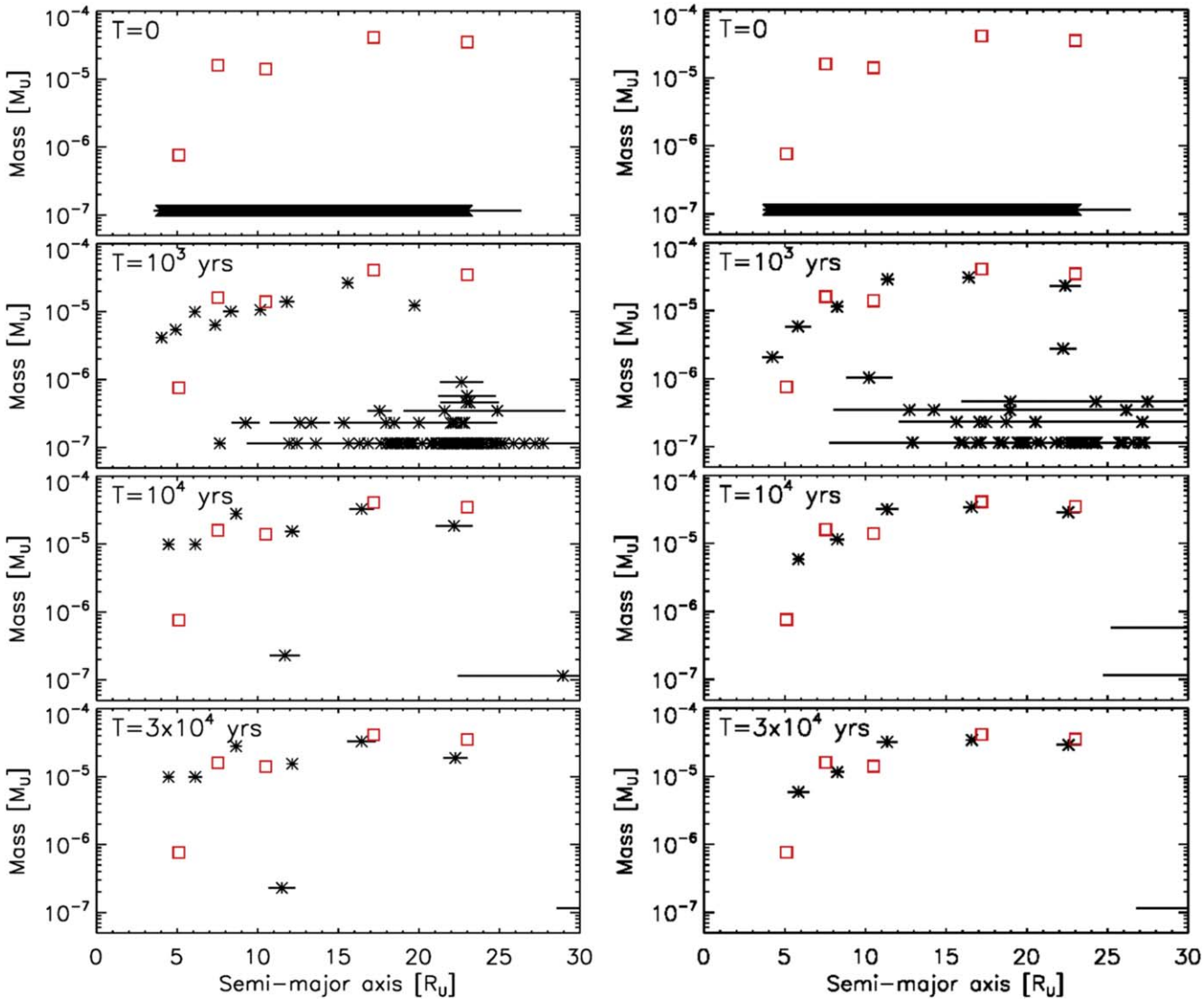

Figure 3. Example satellite accretion simulations. (Left) Evolution of the system from Run 14 in Table 2. The disk is composed of 1000 equal-mass particles (black stars) with a constant surface density profile. The red squares show the current mass and position of Miranda, Ariel, Umbriel, Titania, and Oberon. (Right) Evolution from Run 13 in Table 3 including removal of particles interior to $3R_U$. After 3×10^4 yr, both cases yield distributions of satellites broadly similar to those of the outer four large moons. However, in all of our simulations, the innermost final moon is significantly more massive than Miranda, whose origin may be different.

implying similar bulk compositions with $\geqslant$50% rock by mass, consistent with material expected in a co-accretion disk. In contrast, Miranda's density is $1.17\,\mathrm{g\,cm^{-3}}$. Miranda has Enceladus-like tectonic features, attributed to upwelling of partially melted ices due to past tidal heating (e.g., Pappalardo & Schubert 2013; Beddingfield et al. 2015), and such endogenic activity seems inconsistent with preservation of large-scale porosity in its interior. Thus, Miranda's density seems to imply a much higher ice content than in the large moons, which is difficult to reconcile with an origin from the reaccumulation of material produced during earlier co-accretion. Instead, it is possible Miranda originated from material in the ice-rich c-disk, perhaps consistent with the model of Hesselbrock & Minton (2019); we return to this issue in Section 3.5.

With these caveats, we conclude that reassembly of a disrupted prior satellite system formed by co-accretion could plausibly produce a satellite system resembling the current four large Uranian moons, so long as the pre-impact Uranian obliquity was substantial ($\theta_0 \geqslant 40°$). For the remainder of the paper we focus on what we find to be the more constraining final phase of the co-accretion + giant impact model, in which the inner massive c-disk cools and viscously evolves.

3. Evolution of a Massive C-disk

In this section we consider the evolution of the c-disk to evaluate whether it and its massive byproducts can remain interior to the synchronous orbit and be lost to inward tidal evolution, as was speculated by Morbidelli et al. (2012).

We consider the limiting case of a pure water impact-generated c-disk that is initially completely vaporized. We assume that c-disk vapor has a negligible viscosity and does not radially spread. If the c-disk vapor did viscously spread, a mass much greater than the current Uranian satellites may be transported to the outer disk, yielding excessively massive and ice-rich outer moons (although see Ida et al. 2020). Nearly inviscid c-disk vapor may be plausible. Hydrodynamic turbulence does not appear to produce viscosity (e.g., Ji et al. 2006), and for a late impact after nebula dispersal there would

Table 3
N-body Simulations of Outer Debris Disk Accretion with Removal Inside $3R_U$

Run	N_{sats}	M_{sats} (M_{AUTO})	a_{min} (R_U)	a_{max} (a_{Oberon})	$\langle e_{sats}\rangle$	$\langle i_{sats}\rangle$ (deg)
1	4	1.02	4.88	0.48	0.017 ± 0.004	1.7 ± 1.02
2	4	0.90	4.44	0.42	0.040 ± 0.027	1.6 ± 1.14
3	2	0.47	4.33	0.23	0.012 ± 0.003	3.9 ± 0.10
4	2	0.33	4.32	0.22	0.015 ± 0.007	3.1 ± 0.02
6	5	0.96	5.46	0.74	0.012 ± 0.005	1.2 ± 1.03
9	2	0.44	4.23	0.23	0.036 ± 0.022	2.6 ± 0.72
10	2	0.30	4.35	0.22	0.010 ± 0.002	3.9 ± 0.33
13	4	1.02	8.25	0.98	0.037 ± 0.018	1.0 ± 0.54
14	4	1.10	4.81	0.98	0.047 ± 0.037	1.9 ± 1.23
15	4	0.93	7.55	0.70	0.025 ± 0.008	2.7 ± 0.54
16	4	0.85	5.46	0.53	0.017 ± 0.015	2.7 ± 1.04
17	2	0.62	4.89	0.26	0.026 ± 0.005	5.0 ± 0.44
18	2	0.44	4.87	0.26	0.015 ± 0.007	4.2 ± 0.56
19	4	0.97	7.95	0.87	0.028 ± 0.019	1.5 ± 0.87
20	5	0.98	5.85	0.94	0.019 ± 0.010	1.8 ± 0.69
21	4	1.03	9.26	1.33	0.033 ± 0.018	1.0 ± 0.45
22	5	1.06	5.80	1.22	0.057 ± 0.033	2.5 ± 2.05

Note. Results from a subset of the runs from Table 2 where we have this time removed any particle that passes within $3R_U$ to mimic removal via gas drag from the vapor-rich c-disk.

be no turbulence due to inflowing gas. There is the potential for MRI turbulence because temperatures near $3R_U$ remain >1000 K for $\sim 10^2$ yr after the impact. However, Uranus may not have a dynamo so soon after the impact. In the absence of a planetary field, some simulations of MRI in a vapor protolunar disk find relatively weak viscosities, with a corresponding alpha parameter $\alpha < 10^{-5}$ (Carballido et al. 2016). The effective α in an water-dominated vapor c-disk could be lower still, because it may contain an order-of-magnitude lower abundance of alkali metals (i.e., Na, K) that are the dominant contributors to ionization in the protolunar disk (Carballido et al. 2016). Thus, although it remains uncertain whether the c-disk would spread viscously while in the vapor stage, we assume that it does not, in keeping with the most favorable conditions for the Morbidelli et al. (2012) model.

When Uranus has cooled sufficiently, the water/ice condensation front will move within the Roche limit, located at $a_R = 2.7R_U$ for material with density $\approx 1\ \mathrm{g\ cm^{-3}}$. When water begins to condense within the Roche limit, there will be a viscosity produced as clumps formed by local gravitational instability are continuously sheared apart by planetary tides (Ward & Cameron 1978; Takeda & Ida 2001). This process dissipates energy and causes the disk to spread. For a massive c-disk, the spreading rate will be limited by the disk's ability to cool, through a feedback first recognized in the context of the protolunar disk (Thompson & Stevenson 1988). If the c-disk were completely melt, the rate of viscous dissipation would be so great that it would vaporize the disk. But a vapor c-disk would be gravitationally stable, and as the instability-induced dissipation was deactivated, the disk would cool and recondense, which would reinstate the viscosity. This feedback tends to drive the system to a two-phase melt/vapor state in which the rate of viscous dissipation balances the cooling rate from the disk's vapor photosphere, with (Thompson & Stevenson 1988; Salmon & Canup 2012; Ward 2012; Ida et al. 2020)

$$\frac{9}{4}\sigma\nu\Omega^2 \sim 2\sigma_{SB}T_{ph}^4. \quad (3)$$

The resulting radiation-limited viscosity is

$$\nu \sim \frac{\sigma_{SB}T_{ph}^4}{\sigma\Omega^2}, \quad (4)$$

where T_{ph} is the disk's photospheric temperature. The spreading timescale, $\tau_\nu \sim r^2/\nu$, near the Roche limit for ice with $T_{ph} \sim 200$ K for a water vapor photosphere in a two-phase disk is

$$\tau_\nu \sim \frac{a_R^2\sigma\Omega^2}{\sigma_{SB}T_{ph}^4} \sim 2 \times 10^6\ \mathrm{yr}\left(\frac{\sigma}{6 \times 10^6\ \mathrm{g\ cm^{-2}}}\right)\left(\frac{200\ \mathrm{K}}{T_{ph}}\right)^4. \quad (5)$$

This is some 10^4 times longer than for a two-phase silicate protolunar disk, which has $T_{ph} \sim 2000$ K and $\tau_\nu \sim 10^2$ yr (Thompson & Stevenson 1988; Salmon & Canup 2012; Ward 2012).

C-disk material that spreads beyond the Roche limit or that is placed there directly by the giant impact will accrete into ice-rich moons. An exterior moon interacts with an inner disk through resonant torques that transfer angular momentum from the disk (whose outer edge contracts) to the moon (whose orbit expands; e.g., Goldreich & Tremaine 1982; Charnoz et al. 2010). Modeling the c-disk's evolution requires treatment of both the Roche-interior and Roche-exterior regions and their interactions.

Tidal evolution of moon(let) orbits is also important. We adopt the Mignard tidal model (Mignard 1979, 1980), as in Canup et al. (1999) and Canup & Salmon (2018). Moons interior [exterior] to synchronous orbit spiral inward [outward] due to tides raised on Uranus on a timescale of

$$\tau_{tidal} \sim \frac{Q}{3k_2}\left(\frac{M_P}{m}\right)\left(\frac{a}{R_P}\right)^5\Omega^{-1} \sim 6 \times 10^4\ \mathrm{yr}\left(\frac{Q/k_2}{10^4}\right)\left(\frac{10^{-3}M_U}{m}\right) \times \left(\frac{a}{3R_U}\right)^{13/2}\left(\frac{1.3}{R_P/R_U}\right)^5, \quad (6)$$

where (Q/k_2) are Uranus' tidal parameters, m and a are the moon's mass and semimajor axis, and R_P is Uranus' early radius. The Mignard tidal model quantifies tidal dissipation via a parameter Δt, defined as the time between the tide raising potential and when the equilibrium figure is achieved in response to this potential. The relation between the tidal time lag and the tidal dissipation factor Q is $Q \sim (\psi\Delta t)^{-1}$ for a system oscillating at frequency ψ. For the planet, the dominant frequency is $\psi = 2|\omega - n|$, where ω is the planet's spin frequency and n is the satellite's mean motion, such that $\Delta t \sim 1/(2|\omega - n|\ Q)$.

A central question for the Morbidelli et al. (2012) model is whether moons spawned from the hypothesized massive c-disk could remain interior to synchronous orbit, because if they

were driven beyond $a_{\rm sync}$ by resonant torques and mutual interactions they would survive, and no such massive inner, ice-rich moons exist today. Currently synchronous orbit is at $a_{\rm sync} = 3.25R_{\rm U}$. However per above, early Uranus' radius, R_P would have been somewhat larger than its current mean radius, $R_{\rm U}$. Even a modest difference between R_P and $R_{\rm U}$ is important because (1) the tidal timescale varies as $(R_{\rm U}/R_P)^5$ (Equation (6)), and (2) a more distended Uranus rotates more slowly than the current planet, causing $a_{\rm sync}$ to shift outward to a more favorable early position at $a_{\rm sync} \approx 4.5R_{\rm U}[(R_P/R_{\rm U})/1.3]^{4/3}$. We note that Miranda could initially have been inside $a_{\rm sync}$ and still survive: its small mass implies a tidal evolution timescale longer than the time for $a_{\rm sync}$ to move within its orbit as the planet cools and contracts.

3.1. Numerical Model

We simulate the c-disk using a model developed in the context of the Moon's accretion after a giant impact (Salmon & Canup 2012). Our model represents material within the Roche limit by a uniform surface density disk that is described analytically. Material outside the Roche limit is described by an N-body code (Duncan et al. 1998) modified to include tidal accretion criteria relevant near the Roche limit (Canup & Esposito 1995, 1996). The Roche-interior disk's total mass (M_d) and its outer edge ($R_d \leqslant a_R$) evolve with time due to a radiation-limited viscosity per above and interactions with outer moons. Material that spreads inward onto the planet is removed. As material spreads outward past the Roche limit, we remove it from the continuum disk portion of the model and add it to the N-body code in the form of new moonlets just exterior to the Roche limit. We include the strongest resonant interactions (i.e., the 2:1, 3:2, etc.) for all moons close enough to the disk to have one or more of their strong resonances fall within the disk, i.e., for all moons with a semimajor axis $a < 1.6R_d$, where R_d is the outer radius of the Roche-interior disk. Objects passing close enough to the planet to tidally disrupt (Sridhar & Tremaine 1992) are removed from the N-body code and their mass and angular momentum are added to that of the Roche-interior disk. We consider tidal time delay values $\Delta t = 2.7$ or 270 s, corresponding respectively to $(Q/k_2) \approx 10^4$ or $\approx 10^2$ at a distance of $3.8R_{\rm U}$.

We perform simulations (Table 4) with three different c-disk masses: $M_d = 3 \times 10^{-3}$, 10^{-2}, and $3 \times 10^{-2} M_{\rm U}$. The smallest of these appears insufficient to realign the outer disk to distances consistent with Oberon's orbit (Sections 2.1 and 2.3), but is included here for comparison's sake. For each disk mass, we perform three simulations with different random values for the longitudes of ascending node and mean anomalies of spawned moonlets.

We assume a compact c-disk that initially lies entirely within the Roche limit for material with density ≈ 1 g cm^{-3}. A more extended c-disk is certainly plausible (and perhaps probable), but the compact case appears the most likely to produce a successful outcome in which c-disk material remains interior to synchronous orbit. We consider a non-fully contracted Uranus with a radius of $R_P = 1.3R_{\rm U}$ and rotation period of $\sim$28 hr, so that $a_{\rm sync}$ is shifted outward to $4.5R_{\rm U}$. Finally, we place the four largest moons at their current positions, assuming that they accreted at these locations during the prior debris disk accretion phase (Figure 4).

Table 4
Simulations of the c-disk

Run	$M_{\rm c\text{-}disk}$ ($M_{\rm U}$)	(Q/k_2)	$M_{\rm sats} > a_{\rm sync}$ ($M_{\rm AUTO}$)
1	0.003	10^4	7.45
2	0.003	10^4	6.56
3	0.003	10^4	6.99
4	0.010	10^4	15.19
5	0.010	10^4	15.78
6	0.010	10^4	15.09
7	0.030	10^4	35.20
8	0.030	10^4	40.59
9	0.030	10^4	24.07
10	0.003	100	6.88
11	0.003	100	7.03
12	0.003	100	7.50
13	0.010	100	14.53
14	0.010	100	13.63
15	0.010	100	17.53
16	0.030	100	1.00
17	0.030	100	1.00
18	0.030	100	1.00

Note. Initial parameters and results from simulations of the evolution of a massive c-disk in the presence of analogs for Ariel, Umbriel, Titania, and Oberon (Figure 4). $M_{\rm c\text{-}disk}$ is the mass of the initial Roche-interior c-disk, (Q/k_2) are Uranus' tidal parameters (see text), and $M_{\rm sats} > a_{\rm sync}$ is the total mass of moons beyond $a_{\rm sync}$ at the end of the simulation, in units of the combined mass of the current Uranian moons $M_{\rm AUTO}$. In most cases (Runs 1–15), massive moons spawned from the c-disk expand beyond $a_{\rm sync}$ and disrupt/absorb the outer moons. Only in the case of a very massive c-disk and very strong tidal dissipation in Uranus (Runs 16–18) is the outer moon system retained.

3.2. Cases with Smaller C-disk Masses and Nominal Uranus Tides

Figure 5 shows the evolution of a system with a c-disk of mass $M_d = 0.003M_{\rm U}$. The disk spawns an initial moonlet (orange dot) whose orbit rapidly expands because the resonant interactions with the disk are stronger than the tidal torque from the planet. The moonlet first ceases its outward migration at $\sim 4.25R_{\rm U}$ where its 2:1 resonance lies at the Roche limit. Shortly thereafter, the disk spawns additional moonlets (blue dot). These mostly collide with the first moonlet leading to its growth in mass. However, as some of them get scattered or trapped into mean-motion resonances, they transfer additional angular momentum to the first moonlet whose orbit continues to expand until it crosses the synchronous orbit. Once this first moonlet has receded away sufficiently, a second moonlet can grow and evolve outward through the same process. These accretion dynamics are similar to the continuous, discrete, and pyramidal regimes described in the analytical work of Crida & Charnoz (2012).

After $\sim 1.5 \times 10^5$ yr, the first moonlet spawned from the c-disk absorbs Ariel. After $\sim 4.2 \times 10^5$ yr, it absorbs Umbriel. After 6×10^5 yr, Titania and Oberon have been mostly unaffected, but two very massive interior moons have been brought beyond the synchronous orbit. These would be long lived, and yield a total satellite system mass $\sim$7 times greater than the current system, an unsuccessful result.

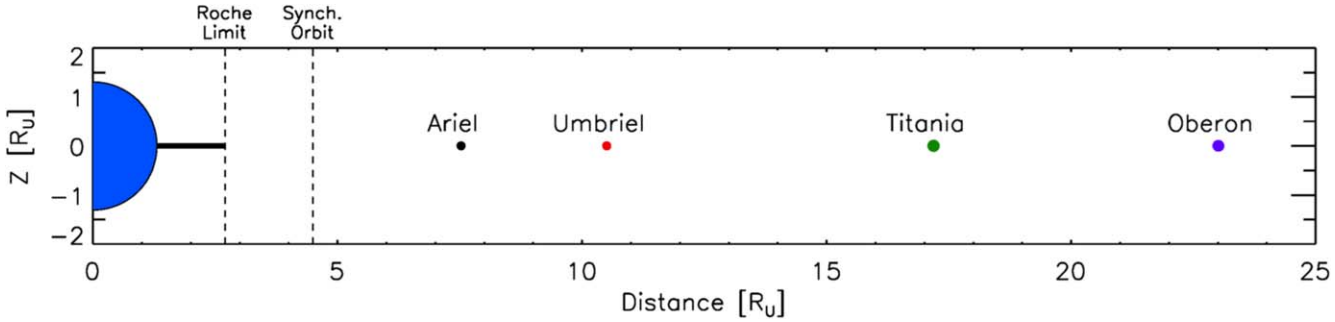

Figure 4. Schematic of our c-disk evolution model. We consider a non-fully contracted Uranus with a radius $R_P = 1.3R_U$ and a rotation period ∼28 hr; for these conditions, synchronous orbit is at $a_{sync} \sim 4.5R_U$ (outer vertical dashed line). An initially compact, water-dominated c-disk extends from the planet's radius to the Roche limit, located at $a_R = 2.7R_U$ for accreting material with density 1 g cm^{-3} (inner vertical dashed line). We place the four largest moons Ariel (black dot), Umbriel (red dot), Titania (green dot), and Oberon (purple dot) at their current positions, assuming that they have successfully reaccumulated from the realigned outer debris disk.

3.3. Cases with Larger C-disk Masses and Nominal Uranus Tides

Figure 6 shows the evolution of a system with a high-mass c-disk with $M_d = 3 \times 10^{-2} M_U$. The disk again spawns a first moonlet (orange dot) whose orbit rapidly expands because the positive resonant toque is much stronger than the negative tidal torque from the planet. However, in this case the first spawned moonlet is massive enough to temporarily confine the c-disk inside the Roche limit, so that for a time $R_d < a_R$. This delays the time until the next moonlet is spawned by the time required for the c-disk to viscously spread back to the Roche limit. After $\sim 2 \times 10^5$ yr, a second moonlet is spawned at the Roche limit and is immediately absorbed by the first one. This repeats twice, until the original spawned moonlet becomes so massive that it perturbs the orbit of Ariel, which is eventually absorbed at $\sim 4.7 \times 10^5$ yr. The dynamical exchange results in the moonlet's new semimajor axis expanding to outside synchronous orbit. After $\sim 4.2 \times 10^5$ yr, the outer three moons go through an instability due to the inner moonlet crossing their mean-motion resonances. This results in Umbriel being ejected from the system.

In this case Titania and Oberon survive at $\sim 6 \times 10^5$ yr, but their orbits have been strongly affected, in particular their eccentricities. Here again, a moon whose mass is $\sim 10 M_{AUTO}$ and is comprised primarily of c-disk material has been brought beyond the synchronous orbit, at odds with the Uranus system.

3.4. Cases with Intense Tidal Dissipation in Uranus

In the previous case we found that a more massive disk can spawn a moon massive enough to confine the disk inside the Roche limit. This limits the number of moonlets produced, resulting in reduced scattering and angular momentum transfer, which keeps the outer system stable for more than $\sim 4 \times 10^5$ yr. However, with weak tidal dissipation in Uranus the large spawned moonlet remains near a_{sync} and does not tidally evolve inward before mutual interactions drive its orbit beyond a_{sync}. As such, we performed a second suite of simulations with the same setup, but with $(Q/k_2) = 10^2$, which produces 100 times faster tidal evolution.

Figure 7 shows the evolution of a system with a high-mass c-disk ($M_d = 3 \times 10^{-2} M_U$) with $(Q/k_2) = 10^2$. A massive moonlet is spawned early on and confines the disk inside the Roche limit while its orbit again rapidly expands to $\sim 4.25 R_U$. But now the tidal torque is sufficient to cause the moonlet to spiral inward before the inner disk can viscously expand back out to a_R and spawn additional moonlets. As the moonlet's orbit contracts, it drives the c-disk toward the planet as well, allowing the outer four satellites to be retained.

3.5. Overall Evolution

As expected based on prior works (Crida & Charnoz 2012; Salmon & Canup 2012; Hesselbrock & Minton 2017, 2019; Canup & Salmon 2018), the most massive moon spawned by a Roche-interior c-disk initially forms near the Roche limit and rapidly recoils via disk torques to a distance $\sim 1.6 r_d$, with $r_d < a_R$ for the initial moon spawned from a sufficiently massive c-disk. Subsequently the disk's edge viscously spreads back out to a_R on timescale τ_ν, which tends to drives the moon outward on this timescale too. The competing effect is tidal interaction with the planet, which so long as the moon remains interior to a_{sync} causes the moon's orbit to lose angular momentum and spiral inward on timescale τ_{tidal}. For the protolunar disk, $\tau_\nu \ll \tau_{tidal}$ and disk accretion produces a moon whose semimajor axis prior to any tidal evolution is ∼2.2 times the Roche limit (Salmon & Canup 2012). This would here imply a massive moon that recoils out to $\sim 6 R_U$ and survives, an unsuccessful result. However, in a water-dominated c-disk, the viscous spreading timescale is orders-of-magnitude longer, and it is possible for very low (Q/k_2) to instead have $\tau_{tidal} < \tau_\nu$. In this case, inward tidal evolution decreases the maximum distance obtained by a spawned moon, keeping it within a_{sync}. Very strong tidal dissipation in early Uranus then provides for a potentially successful outcome, as seen in Figure 7.

In actuality, an inwardly decaying spawned moon will tidally disrupt and resupply the Roche-interior disk, an effect not included in our simulations. On longer timescales the c-disk will continue to viscously spread, lose mass, and spawn ever-smaller inner moons that may be increasingly likely to stay within a_{sync} (Hesselbrock & Minton 2017, 2019). Hesselbrock & Minton (2019) proposed that Miranda (as well as smaller more interior Uranian moons) is a spawned moonlet from a Roche-interior disk with a very low mass, $\sim$few $\times 10^{-6} M_U$. Whether Miranda could originate from the initially vastly more massive c-disk of the Morbidelli et al. (2012) model is an intriguing question. If Miranda did originate from c-disk material, while the 4 large outer moons instead were re-assembled from a prior co-accreted system, this would offer a natural explanation for why Miranda is ice-rich while the outer large moons are $\geqslant$50% rock.

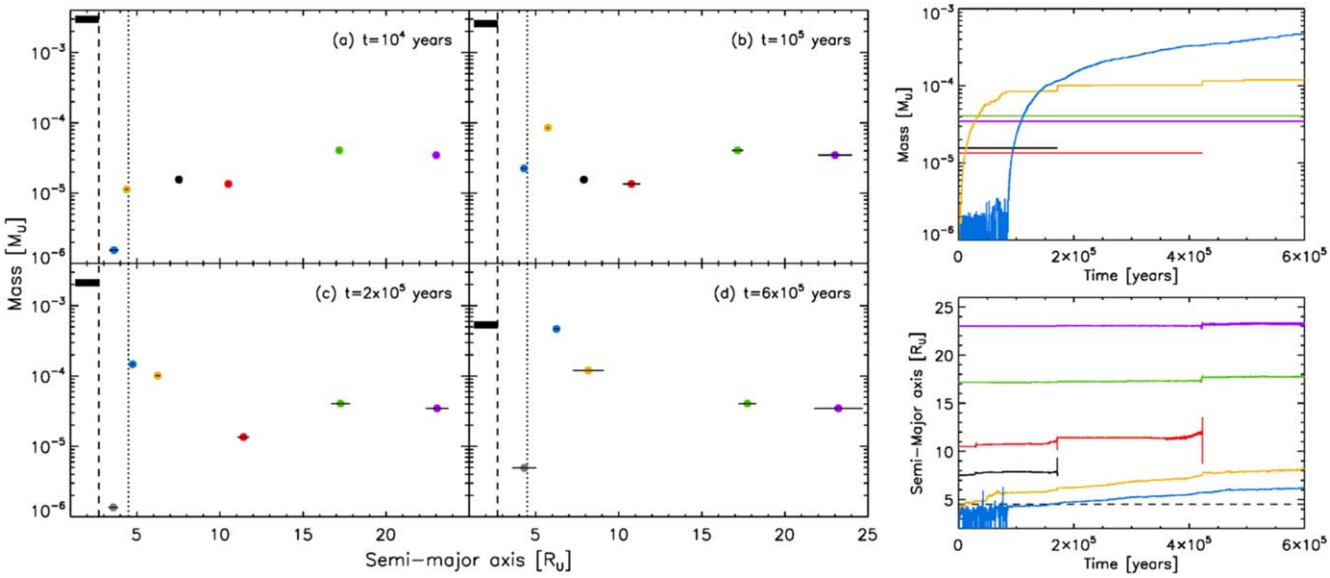

Figure 5. Evolution for a low-mass c-disk with $M_d = 0.003M_U$ and $(Q/K_2) = 10^4$. (Left) Mass and position of the c-disk (black slab) and of the satellites present in the simulation at different times in the evolution. The vertical dashed and dotted lines represent the Roche limit and the synchronous orbit; colored dots show individual moons. The horizontal lines show an object's peri- and apocenter. (Right) Evolution of the mass and semimajor axis of the satellites present in the simulation.

Could Miranda have accreted from the outer portions of a massive c-disk if a low-mass component of the disk initially extended to $\sim 5R_U$? For this to be viable, low-mass Miranda (with mass $10^{-6}M_U$) at $\sim 5R_U$ must avoid being accreted by the much more massive moon spawned at the Roche limit as the Roche-interior c-disk viscously expanded. The simulations shown in Figures 5–7 demonstrate that the first, most massive spawned moonlet has a mass between $\sim 10^{-4}$ and $10^{-3}M_U$ for the Morbidelli et al. (2012) c-disk, and that this moonlet rapidly expands outward to $4.25R_U$ due to disk torques. At this distance, the spawned moonlet would likely dynamically destabilize or accrete Miranda because they would be separated by less than several mutual Hill radii. Broadly analogous results were seen in the Canup & Salmon (2018) simulations of the evolution of an impact-generated disk around Mars: massive Roche-interior disks produced massive spawned moons that accreted and destroyed outer smaller Deimos analogs unless the initial Roche-interior disk mass was below a critical value. Thus, it seems unlikely that Miranda could accrete from the initial outer portions of a massive c-disk and survive.

The second possibility is that Miranda was a spawned moon from the c-disk at a much later stage in its evolution when viscous spreading had reduced its mass by orders-of-magnitude to a few $\times 10^{-6}$ to $10^{-5}M_U$. As the c-disk evolves, it eventually cools sufficiently to completely condense. Once this occurs, the disk's viscous timescale becomes inversely proportional to the square of the disk surface density (Ward & Cameron 1978; Salmon & Canup 2012) and it spreads more and more slowly as its mass progressively decreases. Our code is too computationally expensive to model this protracted spreading evolution. Future simulations using a more dynamically simplified, but computationally efficient model such as that of Hesselbrock & Minton (2019) will be needed to assess whether an initial c-disk massive enough for the Morbidelli et al. (2012) model may, much later in its evolution, spawn a stable Miranda-like moon.

We considered a pure water c-disk because impact simulations indicate that this would be the dominant component for a differentiated rock–ice impactor (Slattery et al. 1992; Reinhardt et al. 2020; Rufu & Canup 2020). The c-disk may also initially contain a minority rock component originating from the impactor's core, which would condense before the water. Its evolution should be less important to the viability of a co-accretion + giant impact model than the evolution of the water because the total mass in rock will likely be much less and because the rock Roche limit is closer to the planet ($<2R_U$), so that rocky moonlets will be more likely than their icy counterparts to remain interior to synchronous orbit and be lost. The c-disk might also contain some gas (H, He) from the outer layers of Uranus that could affect the late inner disk evolution once its water vapor has fully condensed, perhaps via gas drag, before the H-rich component was removed (e.g., via photoevaporation).

4. Discussion

We have explored several aspects of the formation of Uranus' four largest satellites via the scenario proposed in Morbidelli et al. (2012). We assume a Uranus-tipping impact has produced the planet's current $\theta_f = 98°$ obliquity and destabilized a prior satellite system formed by co-accretion, leading to disruptive collisions between the prior satellites and production of an outer debris disk of mass $\sim 10^{-4}M_U$. We first investigated the nodal randomization of the debris disk, including the effect of the postulated inner c-disk produced by the giant impact. We found, in agreement with Morbidelli et al. (2012), that nodal randomization necessary to realign the outer disk with Uranus' post-impact equatorial plane to distances consistent with Oberon requires a c-disk mass $\geqslant 10^{-2}M_U$. This is some 100 times the mass of the current Uranian satellites. The timescale for nodal randomization is of order 10^3 yr.

We then simulated the reaccumulation of the outer debris into satellites. Our *N*-body simulations generally produced an appropriate number and mass of large satellites. However, we show that initial disks with high inclinations and maximum semimajor axes similar to that of current Oberon produce

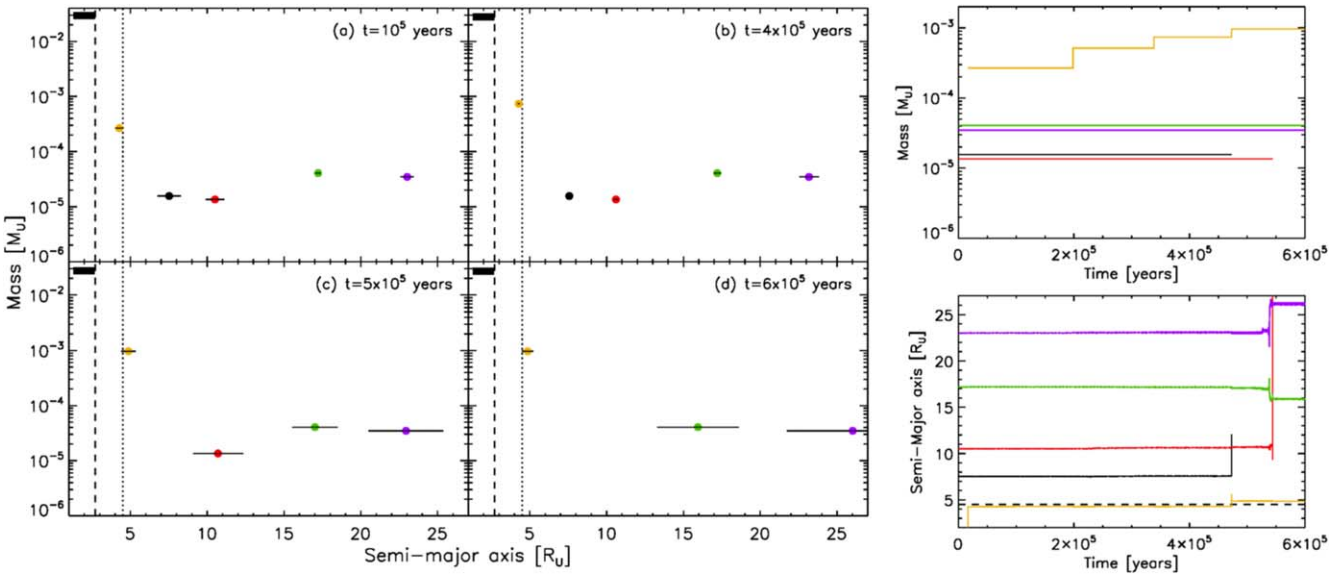

Figure 6. Evolution for a high-mass c-disk with $M_d = 0.03M_{\rm U}$ and $(Q/k_2) = 10^4$. Quantities shown are as in Figure 5.

system that are too compact, with an outermost satellite far interior to Oberon. This is because as the disk collisionally damps, initial debris angular momenta in the equatorial plane tend to cancel out, while the debris angular momentum perpendicular to this plane is approximately retained. Thus, as the initial high-inclination outer debris disk collisionally evolves to form satellites, its outer radius contracts substantially. Accordingly, we identify a new constraint on what the angle between Uranus' pre- and post-impact spin axes, δ, needs to be in the Morbidelli et al. (2012) model to account for Oberon's orbit: $\delta = \cos^{-1}[(25R_{\rm U}/R_{\rm out})^{1/2}]$, where $R_{\rm out}$ is the radius of the prior satellite system. For $(R_{\rm out}/R_{\rm U}) \leqslant 100$ [$\leqslant 50$] δ must be $\leqslant 60^\circ$ [$\leqslant 45^\circ$], implying that Uranus' obliquity before the (final) giant impact must have been large, $\theta_0 \geqslant 40^\circ$ [$> 50^\circ$], a more stringent constraint than previous considered (Morbidelli et al. 2012). An additional mechanism, e.g., a prior giant impact(s) and/or a spin–orbit resonance, is needed to account for θ_0.

Finally, we studied the evolution of a massive, water-dominated inner c-disk as it cools, spreads, and produces new large moons at its outer edge. A c-disk mass of $3 \times 10^{-3}M_{\rm U}$ produces a large number of spawned moonlets because each single one is not massive enough to confine the disk efficiently within the Roche limit. Through scattering and capture in mean-motion resonances, this allows massive spawned moons to gain sufficient angular momentum to expand their orbit beyond the synchronous orbit, which typically destabilizes Ariel and Umbriel after a few $\times 10^5$ yr. The process would result in ice-rich moons interior to Titania and Oberon that are about a factor of 10 times more massive than any moon at Uranus today. For somewhat larger c-disk masses ($\geqslant 0.01M_{\rm U}$), we find that the c-disk produces only one large spawned moon early on, because this moon is massive enough to initially confine the c-disk inside the Roche limit, temporarily shutting off the production of additional moonlets. For nominal tidal parameters for Uranus ($(Q/k_2) = 10^4$), the c-disk eventually viscously spreads back out and produces other spawned moons that result in destabilizing outcomes. However, we found that if tidal dissipation in Uranus was $\sim$100 times stronger than typically inferred, with $(Q/k_2) \leqslant 10^2$, the first moon spawned by a massive c-disk may tidally decay before such destabilization occurs. In this case, the needed evolution in which the c-disk is nearly entirely lost while the outer reaccumulated large satellites are retained may be achieved.

Overall, we find that the co-accretion + giant impact scenario proposed by Morbidelli et al. (2012) is viable, but that it has some very specific requirements. First, the inner c-disk mass must be $\geqslant 0.01M_{\rm U}$, and the inner disk must also remain compact (so that its material does not contaminate the outer moons with too much ice). Whether these conditions are plausible will require further analysis with hydrodynamic impact simulations as is being modeled separately (Rufu & Canup 2020). Second, we identify a constraint between the change in the planet's spin axis due to the impact and the needed outer edge of the pre-impact satellite system. Finally, removal of the ice-rich c-disk and its byproducts appears to require extremely strong tidal dissipation in Uranus for at least the first $\sim 10^6$ yr after the Uranus-tipping giant impact. This is vastly stronger dissipation than current estimates based on properties of the Uranian moons, which estimate that (Q/k_2) averaged over Uranus' 4.5 Gyr lifetime was $10^5 < (Q/k_2) < 10^6$ (with $10^4 < Q < 10^5$ and $k_2 \approx 0.1$; Tittemore & Wisdom 1990) or $1.5 \times 10^5 < (Q/k_2) < 2 \times 10^5$ (with $15{,}000 < Q < 20{,}000$ and $k_2 \approx 0.1$; Ćuk et al. 2020). However, it seems plausible that a much smaller (Q/k_2) could have applied in the aftermath of a Uranus-tipping giant impact, when planet cooling on relatively short timescales could have produced rapid orbital migration via resonance locking (Fuller et al. 2016).

We end with an observation about the timing of a Uranus-tipping giant impact. Uranus' regular satellites currently orbit in a retrograde sense with respect to Uranus' prograde motion about the Sun. If the satellites had acquired their current configuration while the solar nebula was still present, accretion of even a small amount of nebular gas by Uranus would have likely destroyed them because the accreting nebular gas would have produced a circumplanetary disk orbiting in the same sense as Uranus' heliocentric orbit, implying rapid loss via gas drag of satellites orbiting in the opposite sense. Thus, it appears that Uranus satellites must have acquired their current

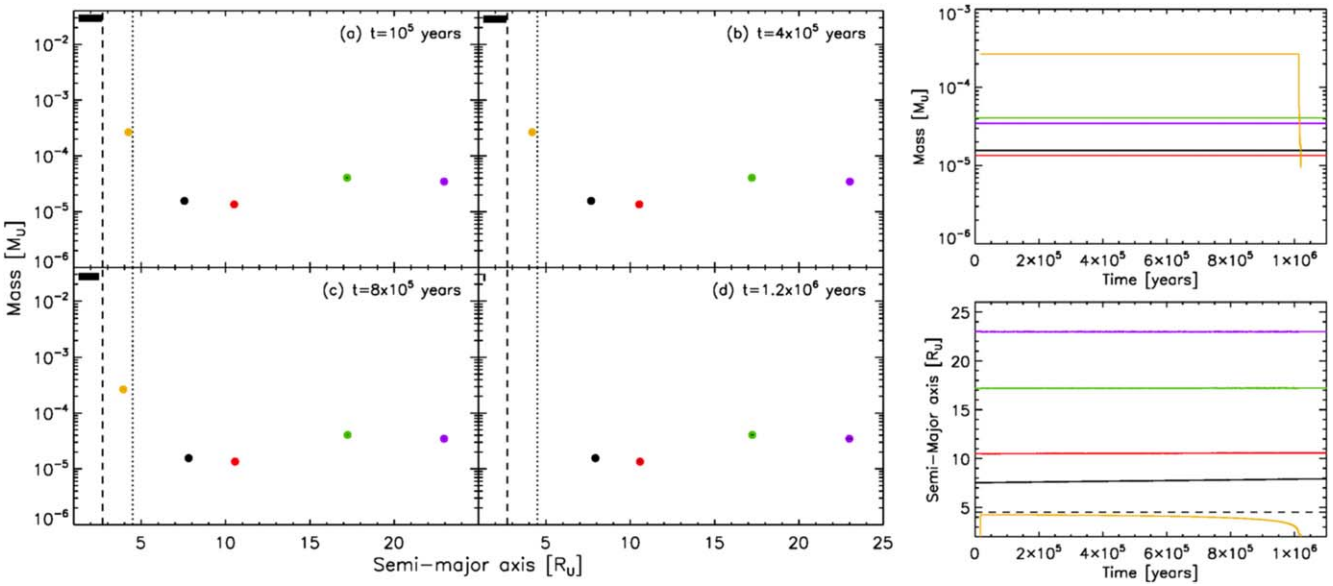

Figure 7. Evolution for a high-mass c-disk ($M_d = 3 \times 10^{-2} M_U$) with strong tides ($Q/k_2$) = 100. The stronger tidal torque causes the first large moon spawned from the c-disk to progressively migrate inward before a second large moonlet is spawned from the disk, eventually falling into the planet and driving the disk inward. The outer satellite system is preserved, a successful outcome.

configuration after the nebula dispersed, which would place the timing of a Uranus-tipping giant impact after nebular dispersal as well.

This work was supported by NASA's Emerging Worlds program grant 80NSSC18K0733.

ORCID iDs

Julien Salmon https://orcid.org/0000-0002-5977-3724
Robin M. Canup https://orcid.org/0000-0002-2342-3458

References

Batygin, K., & Morbidelli, A. 2020, ApJ, 894, 143
Beddingfield, C. B., Burr, D. M., & Emery, J. P. 2015, Icar, 247, 35
Bertotti, B., & Farinella, P. 1990, Physics of the Earth and the Solar System, Geophysics and Astrophysics Monographs, Vol. 31 (Cham: Springer)
Bodenheimer, P., & Pollack, J. B. 1986, Icar, 67, 391
Canup, R., & Salmon, J. 2018, SciA, 4, eaar6887
Canup, R. M., & Esposito, L. W. 1995, Icar, 113, 331
Canup, R. M., & Esposito, L. W. 1996, Icar, 119, 427
Canup, R. M., Levison, H. F., & Stewart, G. R. 1999, AJ, 117, 603
Canup, R. M., & Ward, W. R. 2006, Natur, 441, 834
Carballido, A., Desch, S. J., & Taylor, G. J. 2016, Icar, 268, 89
Charnoz, S., Salmon, J., & Crida, A. 2010, Natur, 465, 752
Cilibrasi, M., Szulágyi, J., Grimm, S. L., & Mayer, L. 2021, MNRAS, 504, 5455
Cilibrasi, M., Szulagyi, J., Mayer, L., et al. 2018, MNRAS, 480, 4355
Crida, A., & Charnoz, S. 2012, Sci, 338, 1196
Ćuk, M., El Moutamid, M., & Tiscareno, M. S. 2020, PSJ, 1, 22
Dobrovolskis, A. R. 1991, BAAS, 23, 1171
Drążkowska, J., & Szulágyi, J. 2018, ApJ, 866, 142
Duncan, M. J., Levison, H. F., & Lee, M. H. 1998, AJ, 116, 2067
Fortney, J. J., Marley, M. S., & Barnes, J. W. 2007, ApJ, 659, 1661
Fujii, Y. I., & Ogihara, M. 2020, A&A, 635, L4
Fuller, J., Luan, J., & Quataert, E. 2016, MNRAS, 458, 3867
Goldreich, P., & Tremaine, S. 1982, ARA&A, 20, 249
Hesselbrock, A. J., & Minton, D. A. 2017, NatGe, 10, 266
Hesselbrock, A. J., & Minton, D. A. 2019, AJ, 157, 30
Ida, S., Canup, R. M., & Stewart, G. R. 1997, Natur, 389, 353
Ida, S., Ueta, S., Sasaki, T., & Ishizawa, Y. 2020, NatAs, 4, 880
Jacobson, R. A. 2014, AJ, 148, 76
Ji, H., Burin, M., Schartman, E., & Goodman, J. 2006, Natur, 444, 343
Lubow, S. H., Seibert, M., & Artymowicz, P. 1999, ApJ, 526, 1001
Mignard, F. 1979, M&P, 20, 301
Mignard, F. 1980, M&P, 23, 185
Morbidelli, A., Tsiganis, K., Batygin, K., Crida, A., & Gomes, R. 2012, Icar, 219, 737
Ogihara, M., & Ida, S. 2012, ApJ, 753, 60
Pappalardo, R. T., & Schubert, G. 2013, LPSC, 44, 2808
Reinhardt, C., Chau, A., Stadel, J., & Helled, R. 2020, MNAS, 492, 5336
Rogoszinski, Z., & Hamilton, D. P. 2020, ApJ, 888, 60
Ronnet, T., & Johansen, A. 2020, A&A, 633, A93
Ruden, S. P., & Pollack, J. B. 1991, ApJ, 375, 740
Rufu, R., & Canup, R. M. 2020, AAS/DPS Meeting, 52, 507.01
Salmon, J., & Canup, R. M. 2012, ApJ, 760, 83
Salmon, J., & Canup, R. M. 2017, ApJ, 836, 109
Shibaike, Y., Ormel, C. W., Ida, S., Okuzumi, S., & Sasaki, T. 2019, AJ, 885, 79
Slattery, W. L., Benz, W., & Cameron, A. G. W. 1992, Icar, 99, 167
Sridhar, S., & Tremaine, S. 1992, Icar, 95, 86
Takeda, T., & Ida, S. 2001, ApJ, 560, 514
Thompson, C., & Stevenson, D. J. 1988, ApJ, 333, 452
Tittemore, W. C., & Wisdom, J. 1990, Icar, 85, 394
Ward, W. R. 2012, ApJ, 744, 140
Ward, W. R., & Cameron, A. G. W. 1978, LPSC, 9, 1205